

The use of X-ray tomography in defining the spatial distribution of barite in the fluvially derived palaeosols of Vaalputs, Northern Cape Province, South Africa



C.E. Clarke ^{a,*}, T.O. Majodina ^b, A. du Plessis ^b, M.A.G. Andreoli ^c

^a Department of Soil Science, Stellenbosch University, P/Bag X1, Matieland, 7602, South Africa

^b CT Scanner Facility, Central Analytical Facilities, Stellenbosch University, P/Bag X1, Matieland, 7602, South Africa

^c School of Geosciences, University of the Witwatersrand, P/Bag 3, Wits, 2050, South Africa

ARTICLE INFO

Article history:

Received 23 February 2015

Received in revised form 11 December 2015

Accepted 13 December 2015

Available online 7 January 2016

Keywords:

Dorbank

Durisol

Duricrust

Duripan

BaSO₄

Palaeosol

ABSTRACT

The distribution pattern of barite in large (15 × 10 × 5 cm) undisturbed aggregates of calcite/clay laminae from a Petric Durisol was investigated using micro-computerised tomography (micro-CT). The petroduric horizons are part of truncated palaeosols which have formed in the Vaalputs sediments located in the Northern Cape Province of South Africa. In these soils clay and calcite laminae encase large polygonal petroduric units. The distribution pattern of barite in relation to the calcite/clay laminae can be used as an indicator to determine the sequence of barite and calcite formation. Samples from two typical profiles were collected for micro-CT analysis. The 2D and 3D visualisation of undisturbed aggregates show an intricate vein network of barite, which runs in a predominantly vertical direction. The barite is intimately associated with the calcite/clay laminae and largely follows the topography of the wavy laminae. In certain instances, along the interface between the petroduric matrix and the laminae, the barite accumulations appear to have wedged the laminae apart. This, together with the unlikelihood that the intricate vein networks of barite would be able to remain intact during the crystallisation of calcite, suggests that barite accumulation in the laminae occurred at the same time or after the calcite laminae were formed.

© 2015 Elsevier B.V. All rights reserved.

1. Introduction

The chemical distribution patterns within undisturbed soil aggregates can be extremely useful in deciphering pedogenic processes. Spatial distribution of chemical components in soils has, in the past, only been successfully achieved with the use of micromorphological techniques, such as energy dispersive X-rays combined with scanning electron microscopy. The resolution of such techniques is very fine and it is often difficult to extrapolate distributions to aggregate or ped scale (centimetre to millimetre scale). In addition these techniques are 2D and thus information is lost regarding the continuity of many chemical distributions.

X-ray tomography, also known as computerised tomography (CT), is an emerging method for 3D geomaterial analysis with many potential applications as reviewed by Cnudde and Boone (2013). In soil science the technique is gaining recognition as it allows non-destructive 3D visualisation of soil components (Tiana et al. 2008). Advances in technology have now made available micro and nano-CT setups for high resolution studies, which are especially useful for investigating pore networks in soils (Sleutel et al. 2008). The micro-CT technique is

particularly useful in determining the spatial arrangement of soil components, soil pore distributions, pore connectivity and related physical properties (Tiana et al. 2008).

The use of micro-CT for the spatial determination of chemical components within soils has not received significant attention. This is largely attributed to the narrow range of molecular weights of soil mineral components. However, when heavy ions are present within the soil matrix, micro-CT analysis can provide a vast amount of information about the 3D spatial distribution of the heavy component. Micro-CT is particularly sensitive to Ba in soils due to its high atomic weight compared to the rest of the soil matrix. This was demonstrated by Brock-Hon and Elliot (2013) in their analysis of petrocalcic materials from the Mormon Mesa in Nevada, USA. In this study Ba, in the form of barite, was shown to clearly contrast from the lower density calcite matrix and highlighted the suitability of micro-CT for observing the distribution of Ba in soil materials. From these observations deductions and confirmations were made about the processes leading to the formation of barite identified in micro-crack infillings.

Barium mobility is limited to specific pedogenic conditions, thus its distribution can be a useful indicator of chemical and hydrological soil processes (Robins et al. 2012). Barium precipitates out of solution in the presence of SO₄²⁻ and CO₃²⁻ ions. Cation exchange sites on clays and organic matter has a high degree of selectivity for Ba over other

* Corresponding author.

E-mail address: cdowding@sun.ac.za (C.E. Clarke).

divalent cations and, due to its size, Ba is often fixed in the interlayer of clay minerals (McBride 1994). These factors can contribute to the low mobility of Ba in soils and Ba redistribution is usually associated with particulate transport (Reid et al. 2005).

The chemical transport and enrichment of Ba requires a sequence of events to occur. Barium must dissolve from a primary or secondary mineral, be transported in solution and precipitate at a location where chemical conditions render Ba insoluble. Carbonell et al. (1999) demonstrated that Ba is soluble under low pH and highly anaerobic conditions in alluvial sediments from the Mississippi River in Louisiana, USA. The proton-promoted and/or reductive dissolution of Mn and Fe oxides adsorbing or co-precipitating Ba were suggested as the main mechanisms for the release of Ba. Release of Ba from barite has been suggested to be related to the microbial reduction of sulphate under anaerobic conditions (Baldi et al. 1996; McCready and Krouse 1980). Stoops and Zavaleta (1978) identified authigenic barite in the subsoil horizons of a Typic Haplustult and associated its formation with hydromorphic conditions caused by saline groundwater. Earlier, Lynn et al. (1971) reported the occurrence of barite in the lower argillic horizons of acidic, aquic subgroups of Alfisols and Ultisols. On the opposite end of the Eh-pH spectrum, the pedogenic barite identified in the Mormon Mesa, occurred in well drained petrocalcic horizons (Brock-Hon et al. 2012). Barium mobility in arid soil systems is less well understood (Brock-Hon et al. 2012) and chemical distributions of Ba can provide important clues as to the mechanism of Ba accumulation and potentially the pedogenic history of ancient soil profiles.

In the Northern Cape Province of South Africa, Ba accumulations have been identified in the petroduric subsoil horizons of the semi-arid Vaalputs palaeosols (Brandt et al. 2005). Little is known about the origin and formation conditions that led to the current morphology of these palaeosols. Micro-CT is an ideal technique for imaging the 3D distributions of Ba in these soils. The Ba distribution patterns would be a useful first step to understanding how the Ba accumulated and how it is related to the soil's history.

1.1. Background to the Vaalputs palaeosols

The Vaalputs palaeosols are derived from Cenozoic fluvial sediments in the semi-arid Vaalputs region of the Northern Cape Province of South Africa (Fig. 1). These sediments, members of the informally defined ~15 m thick Vaalputs formation (Brandt et al. 2005), are a geomorphological anomaly. The deposit characteristics are those of alluvial fan

deposition, but the high ground from which the sediments were derived has been eroded by the slowly retreating Great Escarpment (Brandt et al. 2005; Kounov et al. 2009; McCarthy et al. 1985). As such, the age of these sediments is unknown but they are unlikely to be younger than Early Miocene, i.e. ≥ 15 Ma (Brandt et al. 2005).

Vaalputs lies on the divide between Bushmanland to the east and Namaqualand to the west (Fig. 1). In this region there are numerous silicified mesa-like remnants of the old African erosion plain, which dates to the late Cretaceous (Brandt et al. 2005; Brandt et al. 2003; Partridge and Maud 1987). The Vaalputs sediments themselves are underlain by highly kaolinised saprolite (in this case sandstone of the Dasdap formation (Brandt et al. 2003) and Proterozoic basement rock), characteristic of the ancient planed surface. To the west of Vaalputs rugged outcrops of basement granite-gneiss (Fig. 2) form part of the once elevated Little Namaqua Highland of the marginal escarpment (Mabbut 1955). To the east lies the gently undulating Bushmanland plateau (McCarthy et al. 1985). A second alluvial fan complex, known as the Dasdap sandstones, lies to the south of the Vaalputs sediments, and is comprised of various arenaceous sediments including conglomerate (Brandt et al. 2003; McCarthy et al. 1985). Both the Dasdap and Vaalputs sediments themselves are overlain by sand (thickness ~0.3–1.5 m) which forms hummocky, longitudinal dunes of north-easterly direction (McCarthy et al. 1985; Fig. 2).

Hydromorphic features (i.e. zones of Fe depletions with gleyed colours and yellow and orange Fe mottles) are present throughout the sediments, which may relate to the time of their deposition or humid conditions subsequent to their deposition. Aridification of the west coast of southern Africa took place around 14 Ma and has resulted in large scale silicification and calcification of soils in the region (Partridge and Maud 1987). The current climate of Vaalputs is arid to semi-arid, with an average rainfall of approximately 130 mm/year (Freysen 2014). The dry climate, remote location and thickness of the Vaalputs sediments has resulted in the selection of Vaalputs as the repository for all low level radioactive waste in South Africa (Brandt et al. 2005).

Excavations of large (8 m deep, 8–14 m wide and 20–30 m long) waste disposal trenches within the sediments have exposed a petroduric subsoil horizon (locally known as dorbank), approximately 0.6–0.9 m thick overlain by more recently deposited red sand, approximately 0.2–0.4 m thick (Brandt et al. 2005; Fig. 3). The origin of the overlying sands is uncertain, but has been interpreted by previous workers to be a degraded dune field (McCarthy et al. 1985). At a depth of approximately 1 m, beneath the petroduric horizons, the

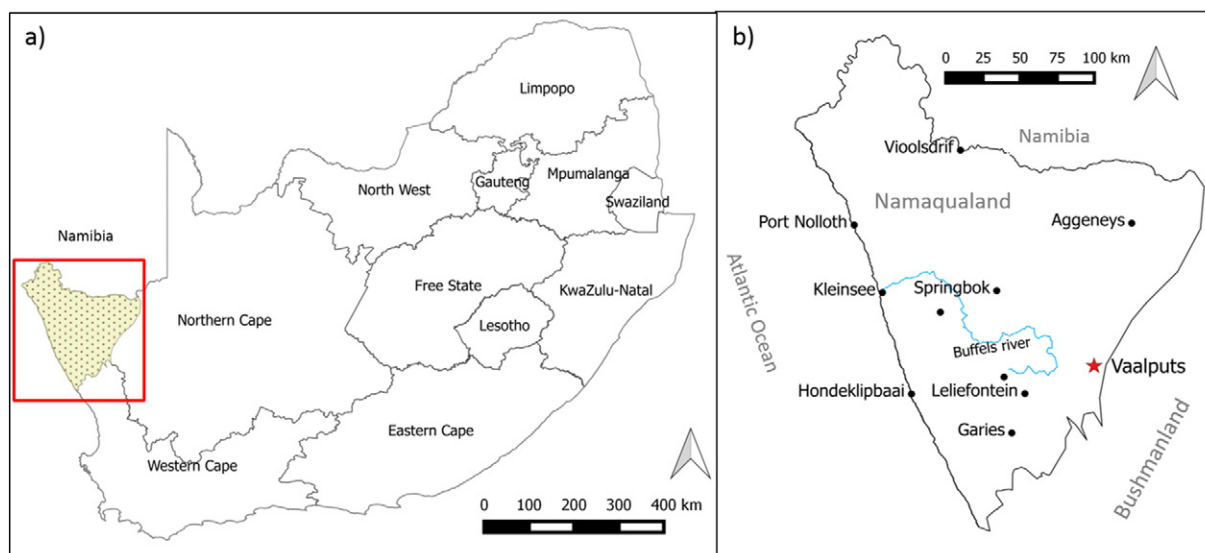


Fig. 1. a) Location of Namaqualand within South Africa (boxed area) and b) location of Vaalputs radioactive waste disposal site within Namaqualand (marked with red star).

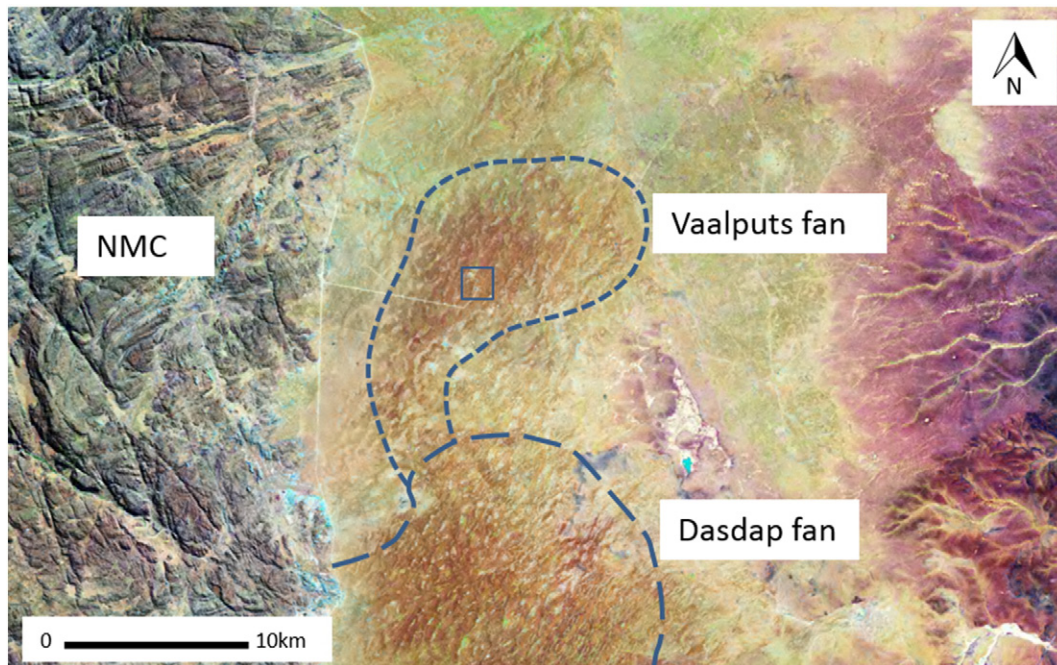


Fig. 2. False colour Landsat image showing the location of the Vaalputs and Dasdap alluvial fan complexes as delineated by McCarthy et al. (1985) covered with hummocky dune structures. Boxed area outlines sampling location. To the west, granite-gneiss outcrops of the Namaqualand Metamorphic Complex (NMC) are exposed by the eastward-retreating Namaqualand escarpment.

top 2 to 3 m of the Vaalputs Formation is poorly consolidated and occasionally impregnated with calcite, gypsum and palygorskite (Andreoli et al. 2014). The covering of sands and a stoneline at the sand-petroduric horizon transition suggest that the petroduric horizon is no longer in phase with current soil forming processes and forms the remnant of a truncated palaeosol. The petroduric horizon is predominantly cemented by silica (slakes in 5 M NaOH), but it contains numerous calcite/clay laminae within and encasing large polygonal ped units (Fig. 4).

Brandt et al. (2005) identified barite in the Vaalputs sediments and pedologically altered petroduric horizons that form part of the truncated palaeosols. Due to the limited envelope of Ba mobility under normal (well aerated, non-saline, non-acidic) soil conditions, Ba distributions in the pedologically altered material can be useful in trying to reconstruct pedochemical conditions of the past. Of particular interest in the Vaalputs soils is the sequence of barite and calcite precipitation in the laminae surrounding the petroduric peds. The hydromorphic features

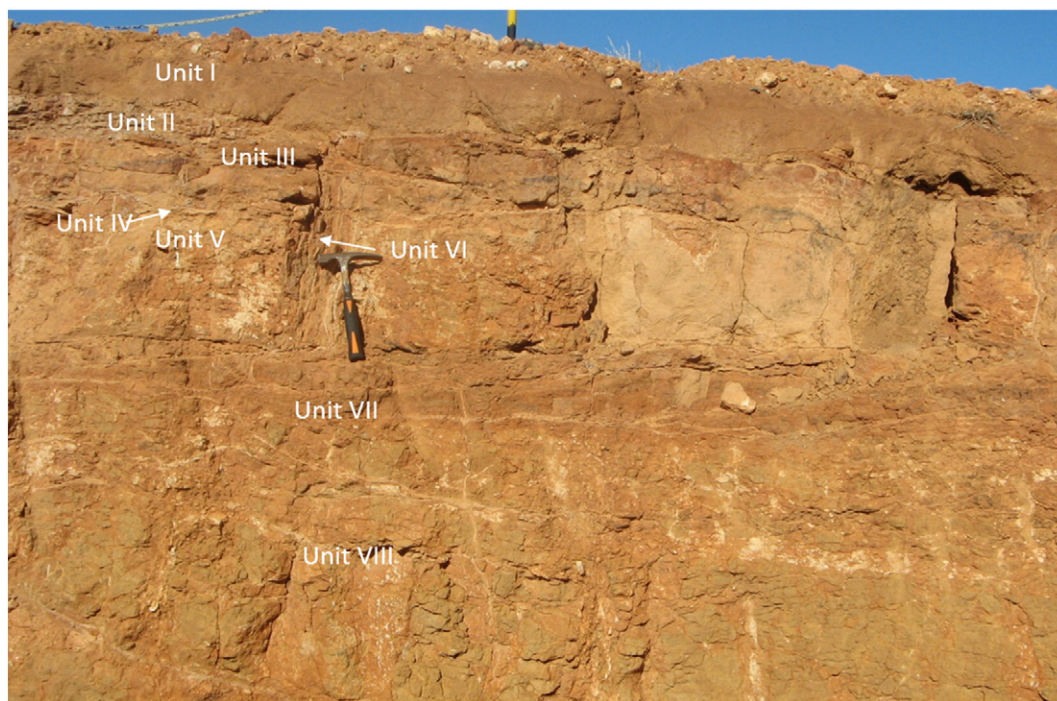


Fig. 3. Soil profile (B11) showing unconsolidated sand (Unit I), medium platy petroduric horizon (Unit II), coarse platy petroduric horizon (Unit III), horizontal clay/calcite laminae (Unit IV), coarse polygonal petroduric horizon (Unit V), vertical clay/calcite laminae (Unit VI), coarse platy petroduric horizon (Unit VII) and poorly consolidated sandy/gravelly, fluvial sediments (Unit VIII).



Fig. 4. a) Example of calcite/clay laminae that envelope large polygonal petroduric units.

in the sediments raise the possibility of Ba redistribution and accumulation under anaerobic conditions, in which case barite accumulation in the laminae would predate aridification. If barite accumulation occurred after calcification, accumulation under arid climates would have to be assumed. Thus understanding the spatial distribution of Ba in relation to the laminae that occur between large polygonal petroduric units can provide clues to the time and conditions of barite formation/redistribution in the pedologically altered material.

The overall aim of this study is to demonstrate the use of micro-CT to establish 3D Ba distribution patterns in undisturbed laminae encasing the large petroduric features of the Vaalputs palaeosols. We then use these distribution patterns to make initial deductions about the sequence of calcite and barite precipitation in the laminae.

2. Materials and methods

2.1. Soil description

Two profiles were selected for analysis and description, one from the walls of trench B 11 (called profile B 11) and the other from the walls of trench C 02 (called profile C 02). The waste disposal trenches are approximately 8 m deep but only the top 2 m were described in detail. Descriptions included: horizon (unit) thickness, field moisture status, dry-state Munsell colour, field texture, structure, degree of induration or consistency, reaction with 10% HCl and transition to the underlying unit. A detailed description of profile B 11 and C 02 are given in Tables 1 and 2, respectively. Traditional master horizon demarcations have been avoided as the horizons of the palaeosol and the current genetic horizons do not correspond (i.e. Unit I represents the current day topsoil and shallow subsoil). The upper petroduric horizons are truncated and not all units described in profile B 11 are present in profile C 02. Although not evident in profile B 11, a stoneline is often present between the red sand (Unit I) and the underlying petroduric horizon suggesting a lithological discontinuity between Unit I and the underlying petroduric horizons. The petroduric units have formed in the Vaalputs sediments. The origin of the sediments is unknown, but clasts of weathered granite-gneiss observed in the lower units of the sediments, suggest the material may have originated from the eroded basement granite-gneiss in the west.

Table 1
Profile description of profile B 11.

Depth (cm)	Description	Sample name
0–20	Slightly moist, dry colour: strong brown (7.5YR 5/6), medium loamy sand, massive apedal structure, slightly brittle consistency; few roots, no HCl reaction, abrupt transition to	Unit I
20–28	Dry, reddish yellow ped interior (7.5YR 6/8) with pink (2.5YR 6/6) cutans/calcanes, medium platy structure, highly indurated (slakes in 5 M NaOH), moderate HCl reaction on clay cutans, abrupt transition to	Unit II
28–50	Dry, red (5YR 5/8), coarse platy structure, gravely coarse sand, highly indurated (slakes in 5 M NaOH), few Mn mottles and cutans around peds, no HCl reaction on cutans, abrupt transition to	Unit III
50–51	Dry, horizontal dense very pale brown (10YR 8/2) and reddish yellow (7.5YR 8/6) laminated material, both pale brown region and reddish yellow laminae have a fine texture, highly indurated moderate HCl reaction, abrupt transition to	Unit IV
51–90	Dry, yellowish red (5YR 5/6) with 40% reddish-yellow (5YR 8/3) mottles, primary structure very large (40–47 cm) block structure, highly indurated (slakes in 5 M NaOH), encased with	Unit V
90–104	Numerous fine (1 mm) very pale brown (10YR 8/2) and reddish yellow (7.5YR 8/6) laminae (band of laminae 3–5 cm wide) showing HCl reaction, abrupt transition to Dry, yellowish red (5YR 5/8), coarse platy structure, gravely coarse sand, moderately indurated and brittle, fine horizontal lamination network system with moderate HCl reaction, abrupt transition to	Unit VII
104–240	Dry, brownish yellow (10YR 6/8), slightly hard, dissected by diagonally intersecting fractures at low angles (<25°), many white (5Y 8/2) coatings on pebbles (– No HCl reaction, positive methyl orange test) at 160 cm depth.	Unit VIII

These soils would classify as Petric Durisols (ruptic) following the World Reference Base (IUSS Working Group WRB 2014) and as a Garies soil form following the South African classification system (Soil Classification Working Group 1991).

2.2. Sample collection

Eleven samples for saturated paste and trace element analysis were collected from each of the major soil units of profile B 11 and C 02 described in Tables 1 and 2.

Table 2
Profile description of profile C 02.

Depth (cm)	Description	Sample name
0–30	Slightly moist, dry colour: strong brown (7.5YR 5/6), medium loamy sand, massive apedal structure, loose consistency; few roots, No HCl reaction, abrupt transition through a stoneline to Dry, mottled yellowish red (5YR 5/6) and very pale brown (10YR 8/3), coarse platy structure, highly indurated (slakes in 5 M NaOH), many hard and fine grained vertical and horizontal pink (7.5YR 8/4) and very pale brown (10YR 8/2) laminae; moderate HCl reaction on laminae, abrupt transition to	Unit I
30–60	Dry, yellowish red (5YR 5/6) with 40% reddish yellow (7.5YR 5/6) mottles, primary structure very large polygonal peds (40–50 cm), highly indurated (slakes with 5 M NaOH) with few cracks and abundant CaCO ₃ mottles (reacts with HCl), many vertical and horizontal very pale brown (10YR 8/2) laminated materials between peds, abrupt transition across the laminae to	Units III and IV/VI (laminae)
60–90	Dry, brownish yellow (10YR 6/6) with 40% yellowish red (5YR 5/8) mottles and 10% white (5Y 8/2) mottles, gravely coarse sand, massive structure, slightly indurated, many white horizontal and vertical CaCO ₃ veins (strong HCl reaction), many coarse fairly rounded gravel fragments.	Unit V and IV/VI (laminae)
90–290		Unit VIII

Prior to the collection of undisturbed laminae for micro-CT analysis, the petroduric horizons were screened for elevated Ba content using a Niton XXt ++ X-ray fluorescence (XRF) portable spectrometer. The highest Ba accumulations were found to occur in the laminated zones (Unit VI) between the large polygonal units of Unit V. Intact laminae samples were collected from this region. Samples were collected by gently separating intact aggregates (roughly $15 \times 10 \times 5$ cm) from the laminated zone. The laminae were extracted easily as they were encased in cutanic material. Extracted laminae were wrapped in packaging tape for transport to the laboratory. A total of eight samples were collected for analyses using micro-CT from the two profiles.

2.3. Mineralogical and micromorphological methods

The mineralogy of the laminated material (Unit VI) and the matrix from the large polygonal petroduric horizon (Unit V) from profile B 11 was determined using X-ray diffraction (XRD). Materials from the sampled reddish yellow (called brown hereafter) and pale brown (called white hereafter) laminations were carefully separated and milled to a fine powder before analysis. The XRD pattern of the milled petroduric horizon had an intense quartz peak, which obscured peaks of other minerals, thus a clay separate was prepared from the crushed portion of the petroduric horizon to concentrate the clay sized minerals. The clay separate was dried and gently crushed into a powder before analysis. All powdered samples were analysed on a Bruker AXS diffractometer using Cu-K α radiation (40 kV and 40 mA) and a V20 variable slit.

Further phase identification was conducted on thin sections prepared from the laminated zones and petroduric matrix. Thin sections were prepared as vertical cross-sections of the laminae. Scanning electron microscopy (SEM) was accomplished using a Zeiss MERLIN FEG® Scanning Electron Microscope with a GEMINI II® column at Stellenbosch University. Prior to analysis the samples were coated with a thin layer of gold in order to establish conductivity. The elemental analyses in spot mode were determined with the backscattered electron detector. The phase compositions of the samples were quantified by energy dispersive spectrometry (EDS) using an Oxford Instruments® X-Max detector and Oxford INCA software. Beam conditions during the qualitative analysis were 20 kV, with a working distance of 12 mm and approximately I-Probe of 16 nA. The counting time was 10 s live-time. The elemental data (in weight %) was normalised to 100%.

2.4. Solution chemistry and total Ba concentrations

Saturated paste extracts were prepared on soil materials from the units of profile B 11 and C 02. Indurated materials were crushed prior to paste preparation. The pastes were allowed to equilibrate for 24 h before extraction under vacuum. Soil pH (Metrohm 905 Titrando) was measured prior to extraction of the soil solution. Electrical conductivity was measured using a Metrohm 905 Titrando. Major cations were measured using a Varian inductively coupled plasma atomic emission spectrometer and anions were measured using ion chromatography with a Metrohm 761 compact ion chromatograph.

Barium concentrations were measured in bulk samples from the units of two profiles (profile B 11 and profile C 02). Samples were milled to pass through a 65 μ m sieve and pressed into pellets. Pellets were analysed using a PANalytical Axios X-ray fluorescence spectrometer.

2.5. Micro-CT analysis

The collected peds were scanned using a commercial General Electric Phoenix (V|Tome|X L240) micro-focus X-ray computed tomography scanner at the Stellenbosch University CT Scanner Facility. All samples were scanned at a voltage and current of 200 kV and 150 μ A, respectively. A 1.5 mm thick copper beam filter was used to produce 80 μ m resolution scans. The resulting data set was reconstructed using the Phoenix Datos |x 2 reconstruction software. Subsequent analyses

were conducted using VGStudio Max version 2.1 and more recently 2.2. Simple thresholding was employed in combination with sharper greyscale gradients over the low density material, to enhance the contrast of the slice images. For detailed observations and analyses, representative subvolumes from each sample were selected and scanned at higher resolutions, the highest being 3 μ m.

Sample analysis using micro-CT involves using grey values to differentiate between the phases in the sample. In a typical analysis, low grey values are indicated by dark regions thus relating to materials of low densities or smaller atomic masses. Conversely, brighter (higher grey values) regions typically relate to higher density or zones of heavier atomic compositions. In the current study, the lowest grey values are represented by the air occurring along surface cracks and within void spaces whereas the brightest zones indicate the distribution of Ba. The segmentation was done based on global thresholding, visualizing all elements heavier than the threshold in the 3D image. This means that other heavy minerals may be visualized in addition to Ba, however EDS analysis of light areas in backscatter SEM imagery, only ever gave a barite chemical signature suggesting that Ba is the only dense phase present. In addition, identification of some of the bright phases on the aggregate surface allowed the use of the Niton XRF analyser on and off the positions of bright phases. In a number of tests, Ba was identified as the only dense phase present.

3. Results

3.1. Mineralogy and micromorphology

The XRD pattern of the clay extract from the petroduric horizon shows illite, kaolinite, quartz and feldspar peaks (Fig. 5). The white laminae show strong calcite peaks, while the brown laminae show illite, kaolinite, quartz and calcite peaks.

In a micrograph of a hand sample (~1 mm) brown laminae are observed between/within the paler calcite laminae (Fig. 6a). Within the laminae, a 7 mm band of coarser textured material, similar to the petroduric matrix is visible. The light microscope thin section micrograph of a vertical cross section of the laminae (Fig. 6b), shows alternating calcite and clay accumulations. The clay accumulations take the form of argillans supporting an illuvial origin.

Barite was not detected in the XRD analysis of either the clay or calcite laminae due to concentrations being below the XRD detection limit (<1 wt%). However, barite was confirmed by SEM analysis of thin sections cut from a vertical cross-section of the laminae (Fig. 7). These images show barite veins within a silica/clay matrix, which was confirmed by EDS analysis (Fig. 7b and c). A high resolution SEM image shows tabular barite crystals between 2 and 4 μ m long (Fig. 7d).

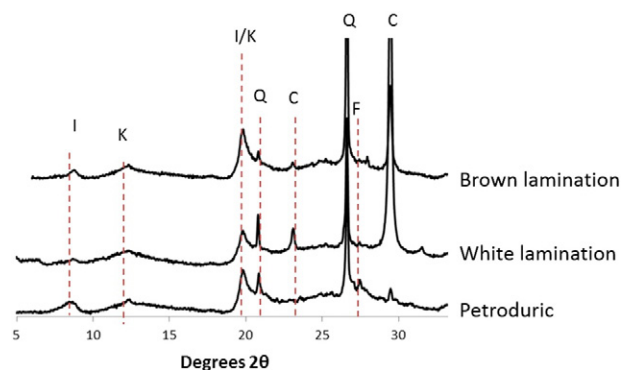


Fig. 5. X-ray diffraction patterns of white and brown laminae (Unit VI) and a clay extract from the petroduric matrix (Unit V) from profile B 11 (I = illite, K = kaolinite, Q = quartz, C = calcite, F = feldspar).

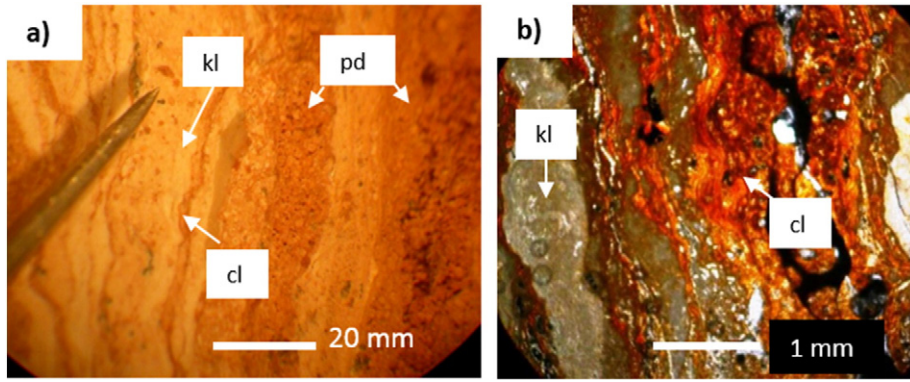


Fig. 6. a) Micrograph of hand sample of vertical laminae (Unit VI; profile B 11) showing calcite (kl), clay (cl) laminae and petroduric matrix (pd); b) thin section micrograph of vertical section through laminae (Unit VI; profile B 11) showing calcite and illuvial clay.

3.2. Micro-CT analysis

Micro-CT analysis of an intact petroduric aggregate from the laminated zone between large polygons is shown in Fig. 8. Fig. 8b and c show that the barite is concentrated in an intricate interconnected vein network while the side view (Fig. 8d) suggests that the vein networks run predominantly parallel to each other in a vertical direction.

Software processing allows visualisation of 2D slices taken throughout the sample (Fig. 9). The calcite laminae are clearly evident in the micro-CT images having whiter values than the clay laminae and petroduric matrix (Fig. 9 b and c). The grey value differentiation made in the images is based on the heavier molecular weight of Ca in relation to Si and Al. The calcite/clay laminae appear to run throughout the aggregate, predominantly in a vertical orientation. From visual

observation of the cross-section, it appears that the laminated zones are less porous and contain fewer quartz sand grains than the petroduric matrix. The thickest zone of calcite laminae occurs on the exterior of the aggregate, including a 1 cm zone of wavy laminae on the horizontal ped surface. The barite vein networks, (shown as white on the images) appear to be associated with the laminae, often following their wavy topography. Virtual slices of a different laminated aggregate are shown in Fig. 10 a–c. The break in the horizontal surface as well as the large void below the bright barite infill gives the impression that barite has wedged the laminae apart.

3.3. Solution chemistry and total Ba concentrations

The saturated paste extract data from major units of B 11 and C 02 profiles are given in Table 3. All horizons, except the red sand show

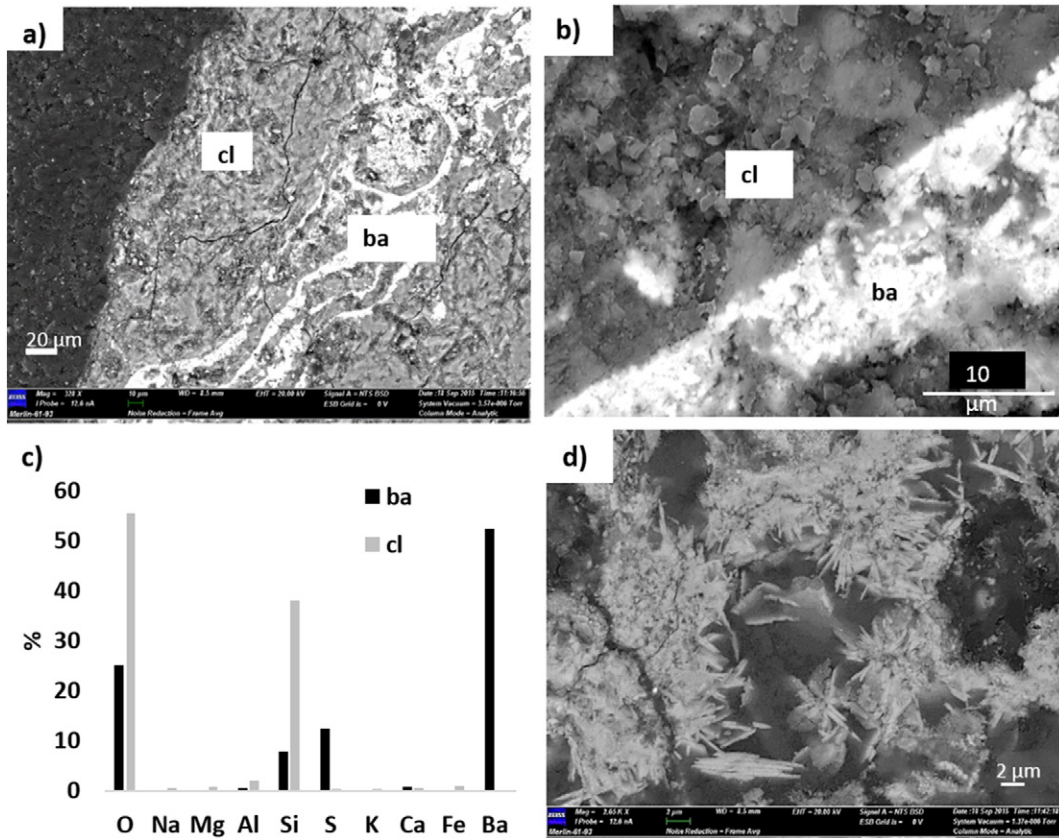


Fig. 7. a) Scanning electron microscope backscatter image of barite veins (ba) within clay laminations (cl) of Unit VI (profile B 11); b) higher resolution backscatter image of the same barite vein; c) semi-quantitative energy dispersive X-ray analysis of clay and barite containing zones; d) backscatter image of tabular barite crystals.

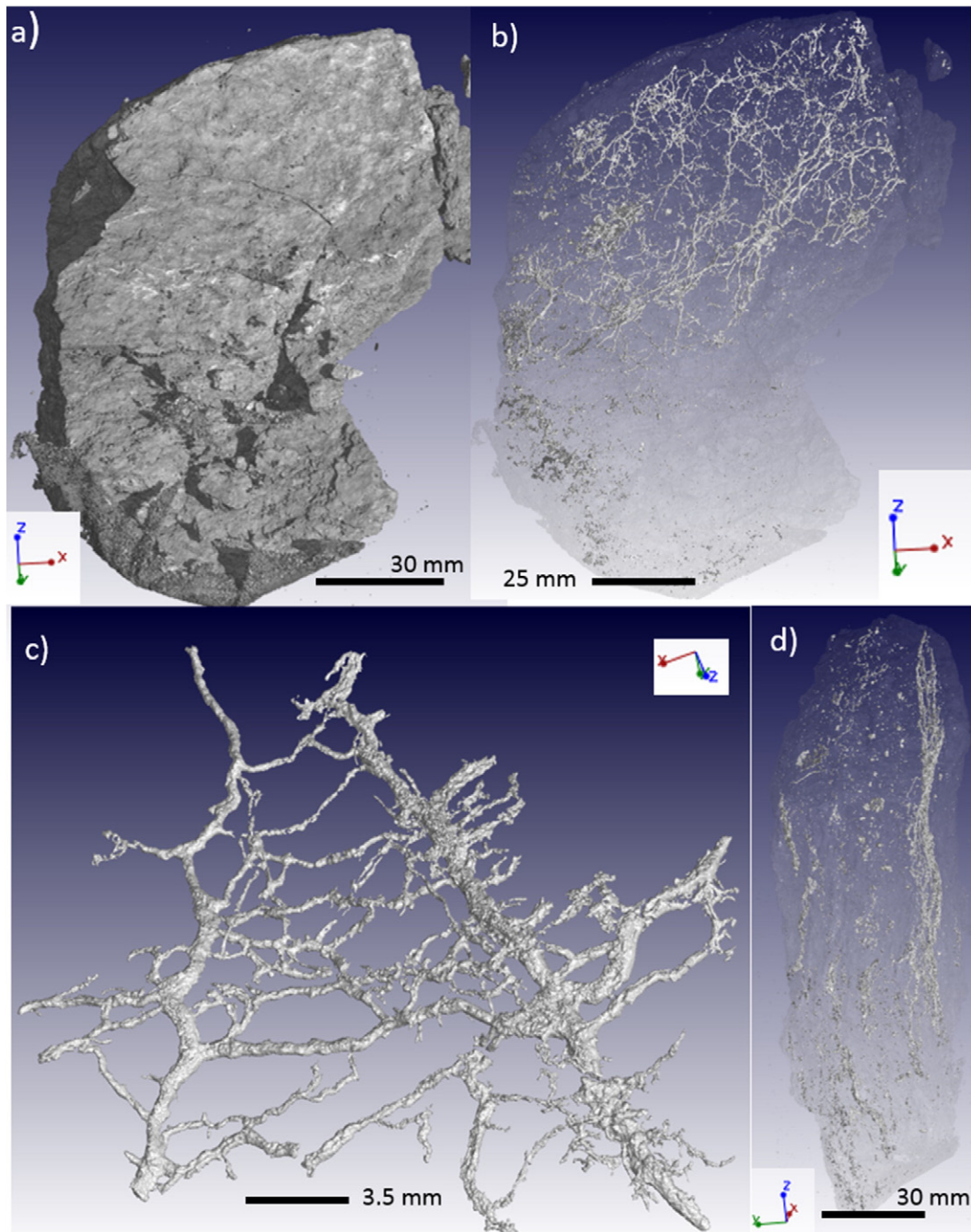


Fig. 8. a) Grey scale image of laminae (white areas show surface accumulations of Ba), b) semi-transparent, 3D view of lamina showing Ba distribution in white, c) enlarged view of vein network, with laminae completely removed and d) side view of laminae showing vertical orientation of Ba vein network.

elevated salinities (226–479 mS/m). The composite laminated zone (including both clay and calcite laminations) shows an extremely high salinity in both profiles. Separate analysis of the calcite laminae from B 11 shows a much lower salinity (412 mS/m). The chemical composition of the saturated paste indicates that Na^+ and Cl^- predominantly contribute to the measured salinity.

Total Ba concentrations of major units from profiles B 11 and C 02 are given in Table 4. In both profiles Unit I shows the lowest concentration of Ba. Elevated Ba concentrations were measured in unconsolidated sediments (Unit VIII) of profile B 11, but such enrichment was not evident in profile C 02. In both profiles the vertical laminated zones show Ba enrichment in relation to the surrounding polygonal units that they encase.

4. Discussion and conclusions

The micromorphological observations suggest that the clay/calcite laminations that coat the large polygonal petroduric structures are likely to be illuvial in nature (Fig. 6a and b). Similar laminae are reported to be present between large polygonal units in the massive petrocalcic horizon of the Mormon Mesa, Nevada (Brock and Buck 2009).

The aggregates used for CT analyses were located in the thick laminated zone (Unit VI) between the large petroduric polygons (Unit V). A wealth of information can be gained from the 2D slices and 3D visualisation of the undisturbed soil aggregates from the Vaalputs soils. The virtual 2D slices in Fig. 9 show that the fine grained calcite/clay laminae are not restricted to the outer walls of the aggregates, but a series of

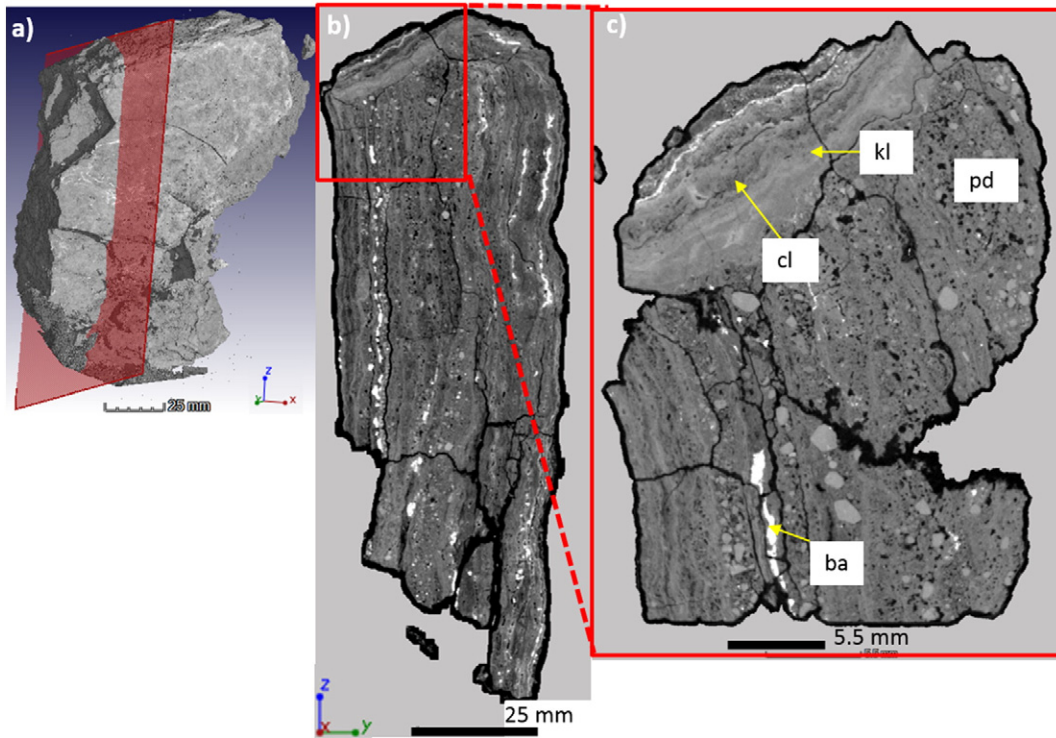


Fig. 9. a) Location of virtual slice of laminated aggregate taken from Unit VI of profile B 11, b) virtual slice of laminae showing distribution of barite (white) in relation to calcite (light grey), aluminosilicate petrduric matrix (dark grey) and void spaces (black) and c) high resolution (3 μm) enlargement of laminae corner (ba = barite, kl = calcite laminae, cl = clay laminae, pd. = petrduric matrix).

laminae occur throughout the aggregate interspersed with more porous and coarser soil matrix material (Fig. 9b and c). A similar alternation between the fine laminae and coarser matrix material is evident in the hand sample micrograph shown in Fig. 6a. The laminae, shown in Fig. 8, occur predominantly in the vertical direction with only the

outer laminae showing horizontal orientation. The formation of these vertical laminae is not easy to explain but is possibly related to the repeated percolation of calcium carbonate and clay laden water into vertical cracks (Bachman and Machette 1977). Precipitation of calcite may have displaced and separated the coarse textured material, as

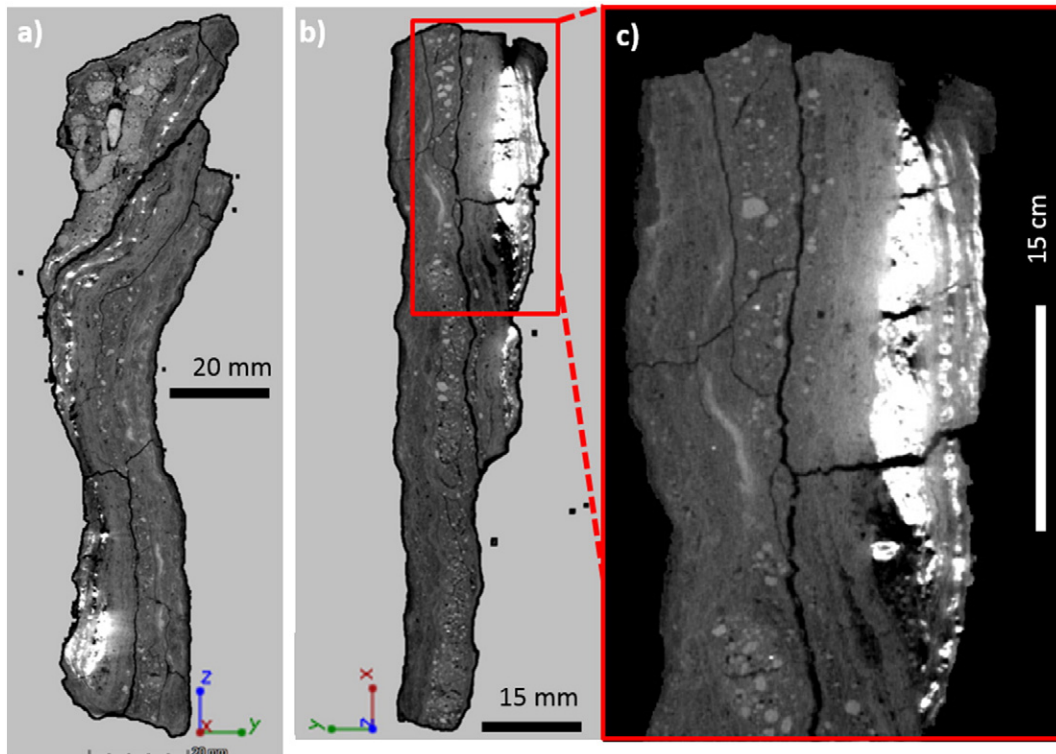


Fig. 10. a) and b) virtual slices taken from two regions of an undisturbed aggregate, c) enlarged view of barite accumulation. Same colour associations are valid as described in Fig. 9.

Table 3
Chemical composition of saturated paste extracts from profiles B 11 and C 02.

Profile	Sample name	pH	EC (mS/m)	HCO ₃ ⁻ mM	F	Cl	NO ₃ ⁻	P	SO ₄ ²⁻	Si	Ca	Mg	Na	K
B 11	Unit I	7.7	54	4.9	0.12	6.82	0.04	BD**	2.31	0.41	1.51	1.63	1.76	7.67
	Unit II	9.2	280	2.2	0.03	BD	0.12	BD	3.84	1.09	1.84	0.56	3.38	1.07
	Unit III	8.2	213	1.7	0.14	57.81	BD	BD	3.77	0.85	8.42	7.06	41.67	1.71
	Unit V	8	429	1.75	0.08	75.42	0.28	0.01	8.58	0.61	6.75	10	43.02	2.18
	Unit VI	7.1	2312	1.65	BD*	282.68	BD	BD	8.21	0.71	32.04	36.77	131.46	5.02
	Unit VI (kl)*	7.8	412	1.83	0.1	46.3	0.38	BD	5.91	3.1	3.73	2.16	10.29	1.26
	Unit VIII	7.8	479	1.75	0.16	88.91	0.33	BD	5.69	8.42	2.29	9.23	64.89	0.63
	Unit I	6.7	42	1.05	BD	1.41	0.08	BD	0.55	0.32	0.31	0.25	1.50	1.13
C 02	Unit III	7.1	814	1.20	0.11	86.28	0.40	BD	7.54	0.59	8.53	17.24	40.87	2.40
	Unit V	7.9	402	1.95	0.21	12.85	BD	0.16	1.84	0.47	3.27	4.57	27.32	1.51
	Unit VI	7.1	974	1.55	0.16	29.35	BD	BD	2.53	0.75	10.23	15.43	58.71	2.86
	Unit VIII	7.4	226	2.45	0.16	49.69	BD	0.81	3.90	0.38	1.36	1.97	16.16	1.26

* kl = calcite laminations which were extracted separately from the bulk laminae.

** BD = below detection limit.

described by Watts (1978), giving rise to the alternating coarse and fine textures observed throughout the peds (Fig. 9b and c). The density and number of laminae around the aggregate exterior suggest numerous illuviation cycles, which under the dry climatic conditions is an indication of the extended time periods involved in forming the morphological features. It is not clear from where the illuvial material originated. Cutans/calcanes are evident on the surface of all petroduric units including Unit II, which lies directly below the non-calcareous sand. This raises the question about the origin of the CaCO₃. In addition to this, clay mobility is limited in the presence of calcareous material (Schaeztl and Anderson 2005), thus the alternating deposition of clay and calcite is not easy to explain, but most likely relates to units that have been eroded from the current petroduric surface.

The ultimate source of Ba in the Vaalputs Durisols is unclear. Robins et al. (2012) postulated that dust is an important source of Ba in arid soils. The low concentrations of Ba in bulk samples from Unit I (Table 4) suggests that an aeolian source is unlikely in the case of the Vaalputs sediments. A more likely source of Ba is the sediments themselves. Brynard (1988) studied the geochemistry of the underlying calcretized sediments and the deeper less calcic sediments. The average values for Ba in the calcretized (18 samples) and lower sediments (32 samples) were 800 and 550 ppm, respectively. The elevated Ba concentrations in the petroduric units and underlying sediments (Table 4) would support a sediment source. Thus it is possible that the Ba was released directly from the chemical weathering of the sediments, however, it is not clear from the available data whether the Ba was originally housed in primary silicates or secondary minerals. In both profiles analysed, Ba is enriched in the laminated zone compared to the petroduric unit in which they have formed (Table 4), which suggests a redistribution within the horizon or translocation from surrounding units.

The barite distribution pattern in relation to the calcite/clay laminae provides clues as to the timing of the Ba redistribution in the Vaalputs soils. The accumulation of barite in a fine vein network (Fig. 8) and the tabular euhedral crystal habits observed during SEM analysis

(Fig. 7d) adds further evidence to the neoformation of barite within the laminae. The vein network also rules out the possibility of Ba accumulations being simply a result of illuvial Ba-enriched clay accumulations.

The intricate vein network also provides clues as to the timing of the barite deposition. The presence of fine intact barite vein networks suggests that there has not been significant movement of the soil since their formation. The crystallisation pressures of calcite precipitation (Watts 1978) and the shrinkage of the soil to form the large polygonal units would have caused significant soil movements during the drying out process. If barite precipitated under wetter soil conditions, it is unlikely that its intricate vein network would have survived these disturbances and would appear more brecciated. In addition, the barite is observed to follow the topography of the calcite/clay laminae and the separation of the laminae from the petroduric matrix in Fig. 10 gives the impression that the laminations have been wedged apart by barite precipitation. This may indicate that Ba-rich solutions intruded the calcite/clay laminae.

If an illuvial mechanism was responsible for the formation of the cutans/calcanes, then the laminae should increase in age from the ped interior to the ped exterior. Barite is observed between outer laminae on the horizontal aggregate surface (Fig. 9c), thus barite precipitation would post-date the formation of the inner laminations. Both the accumulation of barite in vein structures and its intricate association with the laminae suggest that barite precipitation has either post-dated or was at least contemporaneous with the formation calcite/clay laminae.

Based on the chemical distribution patterns observed in the undisturbed aggregates, and substantiated by the euhedral crystal habit of the barite, we propose the barite in the laminae zones precipitated under pedogenic conditions. The close relationship of barite and the calcite/clay laminae would suggest that barite precipitated in the laminated zone largely under arid soil conditions, however, further work would be needed to substantiate this.

Barite redistribution under arid conditions is difficult to explain given its insolubility in carbonate-rich environments. Brock-Hon et al. (2012) identified pedogenic barite in a massive petrocalcic horizon of the Mormon Mesa and suggested that Ba could be mobilised under high salinity during periods of heightened aridity. This builds on evidence that barite solubility increases in the presence of chloride salts (Davis and Collins 1971; Templeton 1960). Robins et al. (2012) provide a number of scenarios whereby barite accumulation may occur in arid environments, these include i) zones of restricted solution flow, ii) sites of increased palygorskite/sepiolite precipitation or iii) horizons reflecting the maximum wetting depth. Fibrous clay minerals are known to occur in the Namaqualand region (Singer et al. 1995) and sepiolite is commonly encountered as coatings on the pebbly material below the Vaalputs petroduric units (Andreoli et al. 2014). Although palygorskite and sepiolite could not be unambiguously identified in

Table 4
Total Ba concentrations of units sampled from profiles B 11 and C 02.

Unit	Profile B 11 (mg·kg ⁻¹)	Profile C 02
Unit I	200	208
Unit II	227	NP*
Unit III	909	803
Unit V	1176	354
Unit VI	2934	8316
Unit VII	217	NP
Unit VIII	4556	355

* NP = unit not present.

the XRD patterns and SEM analysis of the laminated zones, the outer laminae frequently tested positive for sepiolite using a methyl orange indicator (Mifsud et al. 1979). Thus the role of fibrous clays in the precipitation of barite cannot be ruled out.

A salinity induced redistribution of Ba in the Vaalputs palaeosols is another plausible explanation for the current distribution pattern of barite observed in the micro-CT analysis. The saturated paste data (Table 3) show elevated salinities in the laminated zone between the large polygonal features. The reason for this increased salinity is unclear but may relate to evaporative concentration of salts along the macroped faces. Transport of Ba and its precipitation at the evaporative face may therefore also result in the current distribution pattern, but further work would be needed to verify this.

Although there are still many questions that remain about the origin of Ba and how it relates to the pedogenesis of the palaeosols, the 3D imaging of Ba distribution and the internal structure of the laminae has provided the initial step in understanding the system and provided a number of insights that were not possible using high-resolution SEM techniques. Further work on these soils is warranted as understanding the conditions under which they formed will provide valuable insights into the palaeoclimates that shaped the ancient Namaqualand/Bushmanland land surface.

Acknowledgements

We would like to thank the South African Nuclear Energy Corporation (Necsa) and Inkaba ye Africa for financially supporting this work. This is Inkaba ye Africa publication number 119. Comments and ad hoc analytical assistance by M Cloete, C Harris and the Necsa R & D department are gratefully acknowledged. We further thank F.C. DeBeers and J.W.Hoffman, Radiography and Tomography Section of Necsa for technical assistance. The authors also wish to thank W Beukes and staff of the Vaalputs Radioactive Waste Disposal Facility for their generous logistical support during field work.

References

- Andreoli, M.A.G., et al., 2014. Clay Stratigraphy at the Vaalputs Low Level Radioactive Waste Disposal Site, Namaqualand, South Africa, 21st General Meeting of the International Mineralogical Association. Johannesburg.
- Bachman, G.O., Machette, M.N., 1977. Calcic soils and calcretes in the southwestern United States. U.S. Geological Survey Open File Rep. U.S. Gov. Print Office, Washington, D.C., pp. 77–794.
- Baldi, F., et al., 1996. Dissolution of barium from barite in sewage sludges and cultures of *Desulfovibrio desulfuricans*. Appl. Environ. Microbiol. 62, 2398–2404.
- Brandt, D., Andreoli, M.A.G., McCarthy, T., 2005. The Late Mesozoic palaeosols and Cenozoic fluvial deposits at Vaalputs, Namaqualand, South Africa: possible depositional mechanisms and their bearing on the evolution of the continental margin. S. Afr. J. Geol. 108, 271–284.
- Brandt, D., Andreoli, M.A.G., McCarthy, T.S., 2003. Mesozoic fluvial deposits on a rifted continental margin near Vaalputs, Namaqualand, South Africa. S. Afr. J. Geol. 106, 11–16.
- Brock-Hon, A.L., Elliot, T.R., 2013. Three-dimensional investigation of petrocalcic materials: insight into pedogenic processes and future applications. Soil Sci. Soc. Am. J. 77 (4), 1436–1441.
- Brock-Hon, A.L., Robins, C.R., Buck, B.J., 2012. Micromorphological investigation of pedogenic barite in Mormon Mesa petrocalcic horizons, Nevada USA: implication for genesis. Geoderma 179–180 (0), 1–8.
- Brock, A.L., Buck, B.J., 2009. Polygenetic development of the Mormon Mesa, NV petrocalcic horizons: geomorphic and paleoenvironmental interpretations. Catena 77 (1), 65–75.
- Brynard, H.J., 1988. A Petrological and geochemical study regarding the suitability of the Vaalputs radioactive waste disposal facility (Ph.D. thesis Thesis) University of Pretoria (230 pp).
- Carbonell, A.A., Pulido, R., DeLaune, R.D., Patrick Jr., W.H., 1999. Soluble barium in barite and phosphogypsum amended Mississippi river alluvial sediment. J. Environ. Qual. 28 (1), 316.
- Cnudde, V., Boone, M.N., 2013. High-resolution X-ray computed tomography in geosciences: a review of the current technology and applications. Earth-Sci. Rev. 123, 1–17.
- Davis, J.W., Collins, A.G., 1971. Solubility of barium and strontium sulfates in strong electrolyte solutions. Environ. Sci. Technol. 5 (10), 1039–1043.
- Freysen, H., 2014. Climate variability at the Vaalputs site, Northern Cape. Necsa report NLM-REP14/045 (60 pp).
- IUSS Working Group WRB, 2014. World Reference Base for Soil Resources 2014. International Classification System for Naming Soils and Creating Legends for Soil Maps. World Soil Resources Reports No. 106, FAO, Rome.
- Kounov, A., Viola, G., de Wit, M., Andreoli, M.A.G., 2009. Denudation along the Atlantic passive margin: new insights from apatite fission-track analysis on the western coast of South Africa. The Geological Society, London, Special Publications 324, 287–306.
- Lynn, W.C., Tu, H.Y., Franzmeier, D.P., 1971. Authigenic barite in soils. Soil Sci. Soc. Am. J. 35 (1), 160–161.
- Mabbutt, J.A., 1955. Erosion surfaces in Namaqualand and the ages of surface deposits in the south western Kalahari. Trans. Geol. Soc. S. Afr. 58, 13–30.
- McBride, M.B., 1994. Environmental Chemistry of Soils. Oxford University Press, New York.
- McCarthy, T., Levin, M., Moon, B.P., 1985. Geomorphology of the western Bushmanland plateau, Namaqualand, South Africa. S. Afr. Geogr. J. 67, 160–178.
- McCready, R., Krouse, H.R., 1980. Sulfur isotope fractionation by *Desulfovibrio vulgaris* during metabolism of BaSO₄. Geomicrobiol. J. 2, 55–62.
- Mifsud, A., Huertas, F., Barahona, E., Linares, J., Fornes, V., 1979. Test de couleur pour la sepiolite. Clay Miner. 14, 247–248.
- Partridge, T.C., Maud, R.R., 1987. Geomorphic evolution of Southern Africa since the Mesozoic. S. Afr. J. Geol. 90, 179–208.
- Reid, K.D., Reneau, S.L., Newman, B.D., Hickmott, D.D., 2005. Barium and high explosives in a semiarid alluvial system, Ca²⁺ ± on de Valle, New Mexico. Vadose Zone J. 4 (3), 744–759.
- Robins, C.R., Brock-Hon, A.L., Buck, B.J., 2012. Conceptual mineral genesis models for calcic pedants and petrocalcic horizons, Nevada. Soil Sci. Soc. Am. J. 76, 1887–1903.
- Schaetzl, S., Anderson, S., 2005. Soils Genesis and Geomorphology. Cambridge University Press, New York.
- Singer, A., Kirsten, W., Buhmann, C., 1995. Fibrous clay minerals in the soils of Namaqualand, South Africa: characteristics and formation. Geoderma 66, 43–70.
- Sluete, S., et al., 2008. Comparison of different nano- and micro-focus X-ray computed tomography set-ups for the visualisation of the soil microstructure and soil organic matter. Comput. Geosci. 34, 931–938.
- Soil Classification Working Group, 1991. Soil Classification: A Taxonomic System for South Africa. Department of Agricultural Development, Pretoria.
- Stoops, G.J., Zavaleta, A., 1978. Micromorphological evidence of barite neoformation in soils. Geoderma 20 (1), 63–70.
- Templeton, C.C., 1960. Solubility of barium sulfate in sodium chloride solutions from 25Å° to 95Å°C. J. Chem. Eng. Data 5 (4), 514–516.
- Tiana, I.A., Heck, R.J., Elliot, T.R., 2008. Application of X-ray computed tomography to soil science: a literature review. Can. J. Soil Sci. 88, 1–20.
- Watts, N.L., 1978. Displacive calcrete: evidence from recent and ancient calcretes. Geology 6, 699–703.